Calpain drives pyroptotic vimentin cleavage, intermediate filament loss, and cell rupture that mediates immunostimulation

Michael A. Davis[a,b], Marian R. Fairgrieve[a,b], Andreas Den Hartigh[c], Olga Yakovenko[d], Bhargavi Duvvuri[e], Christian Lood[e], Wendy E. Thomas[d], Susan L. Fink[c], and Michael Gale Jr.[a,b,1]

[a]Department of Immunology, University of Washington, Seattle, WA 98109; [b]Center for Innate Immunity & Immune Diseases, University of Washington, Seattle, WA 98109; [c]Department of Laboratory Medicine, University of Washington, Seattle, WA 98195; [d]Department of Bioengineering, University of Washington, Seattle, WA 98195; and [e]Division of Rheumatology, University of Washington, Seattle, WA 98109

Edited by Jonathan C. Kagan, Boston Children's Hospital, Boston, MA, and accepted by Editorial Board Member Ruslan Medzhitov January 18, 2019 (received for review October 29, 2018)

Pyroptosis is an inflammatory form of programmed cell death following cellular damage or infection. It is a lytic process driven by gasdermin D-mediated cellular permeabilization and presumed osmotic forces thought to induce swelling and rupture. We found that pyroptotic cells do not spontaneously rupture in culture but lose mechanical resilience. As a result, cells were susceptible to rupture by extrinsic forces, such as shear stress or compression. Cell analyses revealed that all major cytoskeleton components were disrupted during pyroptosis and that sensitivity to rupture was calpain-dependent and linked with cleavage of vimentin and loss of intermediate filaments. Moreover, while release of lactate dehydrogenase (LDH), HMGB1, and IL-1β occurred without rupture, rupture was required for release of large inflammatory stimuli—ASC specks, mitochondria, nuclei, and bacteria. Importantly, supernatants from ruptured cells were more immunostimulatory than those from non-ruptured cells. These observations reveal undiscovered cellular events occurring during pyroptosis, define the mechanisms driving pyroptotic rupture, and highlight the immunologic importance of this event.

pyroptosis | calpain | vimentin | intermediate filaments | rupture

Pyroptosis is considered a lytic form of inflammatory cell death where cells are permeabilized and physically rupture (i.e., burst) to release proinflammatory and immunostimulatory cytosolic content that stimulates the downstream immune response. Pyroptosis is induced by inflammatory stimuli, including microbial infection, microbial products, cell damage, and metabolic insults, and is dependent on activation of caspase 1 (Casp1) or caspase 11 (Casp4/5 in humans) (for review, see ref. 1). Casp1 is activated by cellular sensing of inflammatory stimuli that activate a number of intracellular receptors, such as nod-like receptor protein 3 (NLRP3), nod-like receptor protein 1 (NLRP1), NLR family CARD domain-containing protein 4 (NLRC4), absent in melanoma 2 (AIM2), and pyrin. Upon activation, these receptors bind and nucleate the self-assembly of the adaptor protein apoptosis-associated speck-like protein containing a CARD (ASC) and Casp1 into the inflammasome, a single supramolecular protein complex that drives autoactivation of Casp1. In contrast, Casp11 is activated by direct sensing of cytosolic LPS. Both activated Casp1/11 cleave gasdermin D (GSDMD), which oligomerizes to form pores in the plasma membrane and permeabilize the cell (for review, see ref. 2). Following permeabilization, pyroptotic cells undergo a characteristic cell swelling and are thought to rupture (3), releasing soluble inflammatory intracellular content, such as ATP, IL-1β, IL-18, high mobility group protein B1 (HMGB1), and lactate dehydrogenase (LDH) (a classic marker of cellular lysis) (4), as well as larger inflammatory content, such as insoluble material, inflammasomes, and nuclei (5, 6).

Before the identification of GSDMD as a pyroptotic pore, early studies suggested that pyroptotic cell swelling and rupture were driven by small caspase 1/11-dependent membrane pores. These pores were thought to permit an influx of water that swelled and ruptured cells like an overfull balloon, in a process called colloid osmotic rupture (3). However, recent studies have demonstrated that GSDMD pores are much larger than initially thought, averaging 22 nm in diameter (7, 8). As such, these pores do not demonstrate ion selectivity and should permit bidirectional flow of ions, proteins, etc. by passive diffusion. Therefore, in isotonic environments, it is unlikely that GSDMD pores could permit an osmotic imbalance that would swell and rupture pyroptotic cells, thus suggesting that osmotic forces could not drive pyroptotic cell swelling and rupture. Despite these observations, cell swelling is a recognized feature of pyroptosis. Notably, at 1 to 2 μm in diameter, ASC specks (inflammasomes) are much too large to move through GSDMD pores, yet they are found in extracellular spaces in vivo in response to inflammatory stimuli (5), suggesting that pyroptotic rupture does indeed occur to facilitate release of cytosolic inflammatory and immunostimulatory macromolecules. Together, these observations imply that additional features of the pyroptotic process likely contribute to the release of inflammatory mediators.

Results

Inflammasome-Induced Cell Swelling Can Occur in the Absence of GSDMD Pore Formation. To evaluate the cellular events surrounding Casp1 activation and GSDMD-mediated pore formation, we first sought to uncouple Casp1 activation from pyroptotic cell death. We utilized CRISPR methodologies to knock out GSDMD in

Significance

Pyroptosis is a form of inflammatory cell death. It is driven by plasma membrane pore formation that is thought to rupture cells through osmotic influx, thereby releasing intracellular content that initiates an inflammatory response to fight acute infection and tissue damage. However, when chronic or unregulated, this process can drive autoimmune disease and cancer. Here, we show that pyroptotic cells do not undergo rupture in culture. Instead, the calcium-dependent protease calpain destroys intermediate filaments, which provide mechanical resilience to cells. As a result, cells are susceptible to rupture by mechanical disruption from shear stress or compression as occurs in the blood stream or within tissues. Thus, our data reveal potential targets for the therapeutic intervention of autoimmune diseases and cancer.

Author contributions: M.A.D., C.L., W.E.T., S.L.F., and M.G. designed research; M.A.D., M.R.F., A.D.H., O.Y., B.D., and C.L. performed research; M.A.D. analyzed data; and M.A.D. and M.G. wrote the paper.

The authors declare no conflict of interest.

This article is a PNAS Direct Submission. J.C.K. is a guest editor invited by the Editorial Board.

[1]To whom correspondence should be addressed. Email: mgale@uw.edu.

This article contains supporting information online at www.pnas.org/lookup/suppl/doi:10.1073/pnas.1818598116/-/DCSupplemental.

Published online February 22, 2019.

human THP-1 monocytes. For comparison, we also knocked out NLRP3, ASC, and Casp1. Multiple different guide RNA (gRNA) were tested for each gene, and subsequent results were confirmed with at least two functional gRNA for each. Knockout was verified by immunoblot analysis (Fig. 1*A*). To verify that knockout prevented pyroptotic cell death (i.e., permeabilization and cell swelling), we activated the NLRP3 inflammasome in THP-1 cells with nigericin (Ng) treatment and assayed cell permeabilization through uptake of Sytox-Green (Sytox), a cell-impermeable nucleic acid stain (Fig. 1*B*). While WT cells reached complete permeabilization within 2 to 3 h after Ng treatment, NLRP3 and ASC knockouts were fully resistant to Ng-induced cell death. However, GSDMD loss only delayed cell death, and the cells died with similar kinetics to ΔCASP1 cells. These observations are consistent with reports demonstrating that, in response to inflammasome activators, both Casp1 and GSDMD knockouts die in a delayed fashion through a Casp8-mediated apoptosis (9–12).

Surprisingly, unlike ΔNLRP3 or ΔASC cells, both ΔCASP1 and ΔGSDMD cells were as swollen as WT cells at 3 h post-Ng treatment (Fig. 1*C* and *SI Appendix*, Fig. S1). However, at this time point, swollen ΔCASP1 and ΔGSDMD cells were largely Sytox-negative and thus not permeabilized, as might have occurred through cleavage of other gasdermin family members (13). Moreover, quantification of swelling over time revealed that cell swelling was delayed in both Casp1 and GSDMD knockouts (Fig. 1*D*) and that Ng-induced swelling in both ΔCASP1 and ΔGSDMD cells was blocked when they were treated with the pan-caspase and calpain inhibitor Z-VAD (Fig. 1*E*). Together, these results demonstrate that inflammasome-dependent cell swelling can occur in a delayed fashion in the absence of Casp1 or GSDMD. Importantly, these data indicate that Z-VAD–sensitive enzymatic events within the cell may drive cell swelling during pyroptosis following cell permeabilization.

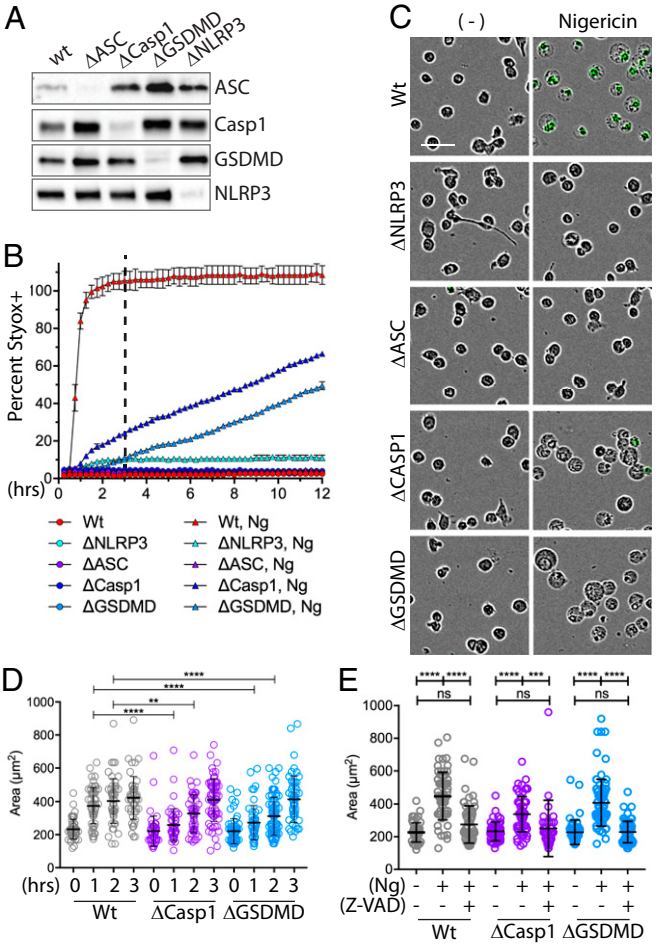

Fig. 1. Inflammasome-stimulated cell swelling occurs in the absence of Casp1 and GSDMD. (*A*) CRISPR methodologies were used to knockout ASC, Casp1, GSDMD, or NLRP3 in THP-1 cells. Knockout was verified by immunoblot analysis. (*B*) Wt, ΔNLRP3, ΔASC, ΔCasp1, or ΔGSDMD THP-1 cells were treated with Sytox ± Ng. The number of Sytox-positive cells (i.e., dead cells) was quantified over time via IncuCyte analysis. Error bars show SD of triplicate wells. (*C*) Images from *B* at 3 h after addition of nigericin (dashed line in *B*). (Scale bar: 50 μm.) (*D*) Cell swelling as a function of time after Ng treatment was quantified from IncuCyte images using ImageJ/FIJI. At least 50 cells from a field of view were analyzed. Statistics were calculated via one-way ordinary ANOVA. (*E*) Wt, ΔCasp1, or ΔGSDMD THP-1 cells were treated and analyzed as above, except cells were also treated with the pan caspase inhibitor Z-VAD as indicated. Images from 3 h posttreatment were used. $^{**}P < 0.05$, $^{***}P < 0.005$, $^{****}P < 0.0001$; n.s., nonspecific.

Pyroptotic Cells Do Not Rupture in Vitro. Pyroptotic cells are widely understood to undergo osmotic lysis following GSDMD-mediated permeabilization of the plasma membrane. As a result, pyroptotic cells are thought to rupture, which is defined as a bursting event, such as when a balloon ruptures after being filled beyond capacity. Importantly, this process is distinct from release of cytosolic content and uptake of cell impermeable dyes via diffusion through permeabilized cells with otherwise intact plasma membranes. The idea of pyroptotic rupture is based on landmark findings by Fink and Cookson (3) and has been supported by numerous reports demonstrating rapid uptake of cell-impermeable dyes and release of cytosolic content, such as IL-1β, IL-18, and LDH by immunoblot analysis, ELISA, etc. (14–17). However, reports that document pyroptotic rupture using live-cell imaging equated rupture with uptake of cell-impermeable dyes or release of cytosolic content yet show no evidence of bursting (14, 18, 19). Consistent with these live-cell studies, we observed stable, swollen pyroptotic cell corpses many hours after initial permeabilization, without apparent rupture (Fig. 1*C*).

To more fully examine the process of pyroptotic swelling and rupture, we visualized pyroptotic macrophages by high-resolution, live-cell microscopy. Remarkably, Ng treatment resulted in THP-1 cell swelling without rupture, even 8 h post-Ng treatment (Fig. 2*A* and Movie S1). As pyroptotic cells are reported to undergo osmotic lysis (i.e., water-driven bursting), we then compared pyroptosis to true osmotic lysis and treated THP-1 cells with water (Fig. 2*A* and Movie S2). Unlike pyroptotic cells, water-treated cells ruptured violently, demonstrating that pyroptosis is qualitatively distinct from osmotic lysis. Next, we verified that Ng treatment caused THP-1 cell permeabilization and treated THP-1 cells expressing cytosolic mCherry with Ng in the presence of Sytox. As expected, Ng-treated cells swelled coincident with loss of cytosolic mCherry and uptake of Sytox (Fig. 2*B* and Movie S3), and, consistent with our observations in WT THP-1 cells, pyroptotic mCherry-expressing cells did not burst. To define the breadth of this phenotype beyond the THP-1 human tumor cell line, we repeated these studies in primary human and murine cells. As in THP-1 cells, LPS and Ng-treated human monocyte-derived macrophages (hMDMs) swelled without bursting over a course of 8 h (*SI Appendix*, Fig. S2). Similarly, primary murine bone marrow-derived macrophages (BMDMs) treated with LPS and Ng in the presence of Sytox swelled coincident with uptake of Sytox yet did not burst (Fig. 2*D*).

Glycine can prevent cell swelling and LDH release in pyroptotic J744A.1 murine macrophage cells, as well as LDH release from pyroptotic BMDMs (12, 20–22). Thus, glycine is thought to prevent pyroptotic rupture. However, we found that glycine did not prevent swelling of pyroptotic THP-1 cells (*SI Appendix*, Fig. S3*A*), which is consistent with observations of pyroptotic swelling in BMDMs (19). We also found that glycine does not prevent release

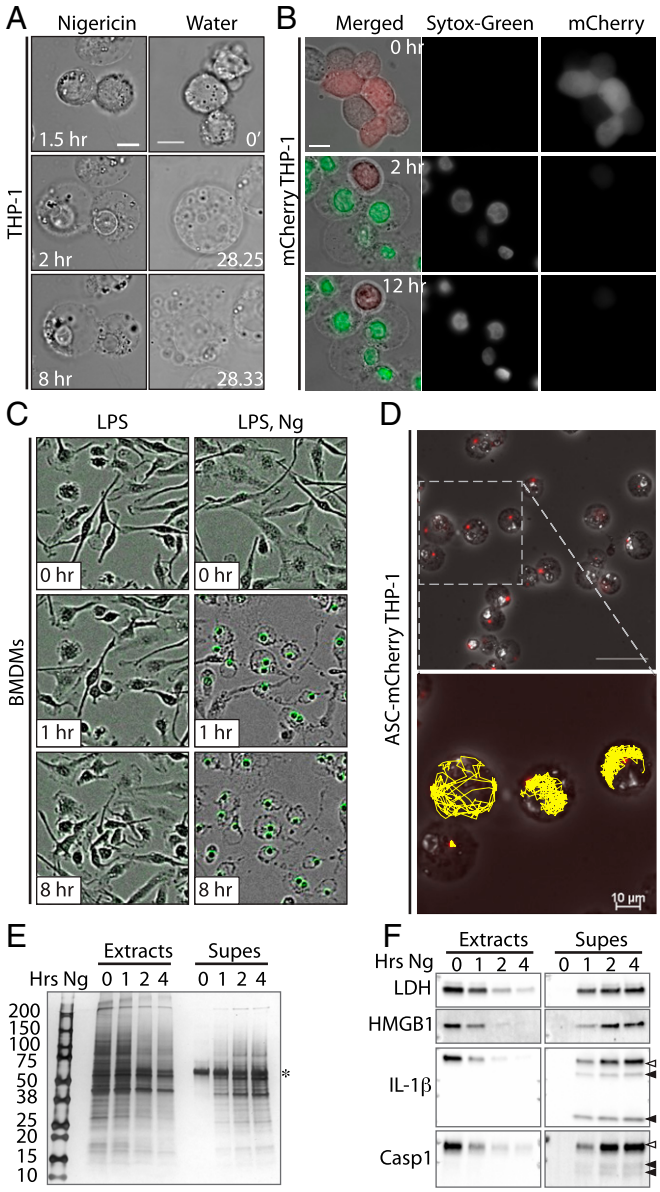

Fig. 2. Unperturbed pyroptotic cells do not rupture in vitro. (*A*) THP-1 cells were treated with Ng and imaged every 30 s for 8 h (Movie S1), or THP-1 cells were treated with water and imaged every 5 s (Movie S2). (Scale bars: 10 μm.) (*B*) mCherry-expressing THP-1 cells were treated with Ng plus Sytox and imaged every 30 s (Movie S3). (Scale bar: 10 μm.) (*C*) BMDMs were treated with LPS/Ng plus Sytox and imaged via IncuCyte. (*D*) ASC.mCherry expressing THP-1 cells were treated with Ng and imaged every minute for 8 h (Movie S4). (Scale bar: *Upper*, 50 μM.) Inflammasome paths were traced in 2D using the TrackMate plugin of ImageJ/FIJI (*Lower*). (*E*) THP-1 cells were treated with Ng in serum-free medium as indicated. Cell extracts and supernatants (Supes) were evaluated by silver stain analysis. Numbers 200–10 indicate molecular weights of ladder bands. The * indicates likely BSA from residual serum. (*F*) THP-1 cells were treated as in *E* and analyzed by immunoblot for indicated proteins. Open and closed arrowheads indicate full-length and cleaved proteins, respectively.

of LDH, IL-1β, or HMGB1 from pyroptotic THP-1 cells (*SI Appendix*, Fig. S3 *C*, *E*, and *F*) although it does affect release of NLRP3 and cleaved vimentin (see below) (*SI Appendix*, Fig. S3*C*). Moreover, silver stain gel analysis of culture supernatants demonstrated that glycine has no effect on the vast majority of protein released from pyroptotic THP-1 cells (*SI Appendix*, Fig. S3*D*), suggesting that the effect of glycine on protein release is protein-specific. Finally, in a side-by-side comparison, we showed that glycine prevents LDH release from BMDMs but not THP-1 cells (*SI Appendix*, Fig. S3*F*), suggesting that the effects of glycine on protein release are also cell type-specific. Thus, glycine cannot be used as a general protectant against pyroptotic rupture.

ASC specks are found in extracellular spaces in vivo (5), which presumably requires a cell to rupture for ASC-speck release. To determine if ASC specks escape pyroptotic cells in vitro, we visualized cells expressing mCherry-tagged ASC by live-cell microscopy. Upon Ng treatment and before cell swelling, mCherry-tagged ASC aggregated to form an inflammasome. However, ASC specks were not released from the swollen pyroptotic cells (Fig. 2*D* and Movie S4). Moreover, ASC specks were retained inside the cells despite the fact that they were quite mobile within the pyroptotic cells, indicating that speck release was not prevented by the cytoskeletal or other potential tethers. Although we cannot rule out the possibility that small tears in the plasma membrane exist to facilitate release of cytoplasmic content, our data argue against large (1 to 2 μm) tears in an otherwise stable and intact plasma membrane.

As mCherry-ASC aggregation in Ng-treated cells demonstrates inflammasome activation, we next verified that these swollen, unruptured cells were fully pyroptotic and released cytosolic content. THP-1 cells were treated with Ng for 0, 1, 2, or 4 h, and we assayed cell lysates and culture supernatants by silver stain (Fig. 2*E*) or by immunoblot (Fig. 2*F*). Silver stain analysis showed a gradual, time-dependent appearance of proteins from >200 kDa to <15 kDa in the culture supernatant. Further, immunoblot analysis demonstrated a time-dependent cleavage and activation of Casp1, as well as cleavage of the Casp1 substrate IL-1β. We also observed a time-dependent release of LDH, HMGB1, cleaved IL-1β, and cleaved Casp1 into the supernatants of Ng-treated cells. These data demonstrate that swollen, unruptured cells indeed release some pyroptotic content.

Together, these data demonstrate that pyroptotic cells do not rupture in vitro and are consistent with a model whereby pyroptotic release of cytosolic content like IL-1β, HMGB1, and LDH occurs by passive diffusion through GSDMD pores, which are wide enough to permit egress of even large proteins and protein complexes (refs. 7 and 8; https://cdn.rcsb.org/pdb101/molecular-machinery/).

The Cytoskeleton Is Disrupted and Lost During Pyroptosis. Our data suggest that cytoplasmic events drive pyroptotic cell swelling. Since the principle regulator of cell shape and integrity is the cytoskeleton (23), we assessed the integrity of the cytoskeleton in pyroptotic cells. THP-1 cells were treated with Ng to activate the NLRP3 inflammasome. We then used immunofluorescence analysis to assess the cytoskeleton in pyroptotic cells, marked by the presence of an ASC speck and/or a condensed nucleus (both hallmarks of pyroptosis) (24). Indeed, inflammasome formation coincided with a catastrophic loss of the microtubule network, as visualized by the loss of α-Tubulin (Fig. 3 *A* and *E*). Inflammasome formation also dramatically disrupted the cortical actin network (Fig. 3 *B* and *E*), as well as cytosolic and nuclear intermediate filaments as visualized by staining for vimentin (Fig. 3 *C* and *E*) and lamin B1 (Fig. 3 *D* and *E*), respectively. Moreover, these cytoskeletal dynamics were quantified temporally, revealing that cytoskeletal disturbances increased over time and correlated with pyroptosis.

To determine if cytoskeletal loss is a general phenomenon of inflammasome-driven pyroptosis or just restricted to NLRP3 activation in THP-1 cells, we first assessed the effects of NLRP3 activation in LPS/Ng-treated BMDMs. Similar to THP-1 cells, LPS/Ng-dependent inflammasome activation in BMDMs led to a loss of microtubules, actin, and intermediate filaments and to a disruption of nuclear lamina (Fig. 4*A*). Similar results were also obtained in primary human MDMs (Fig. 4*C*) although, instead of complete vimentin loss, vimentin staining went from filamentous to punctate, which is similar to what is seen during apoptosis (25). We also infected primary BMDMs with *Salmonella typhimurium*, a human pathogen that causes acute gastroenteritis and activates the NLRC4 inflammasome. As above, treatment of BMDMs with

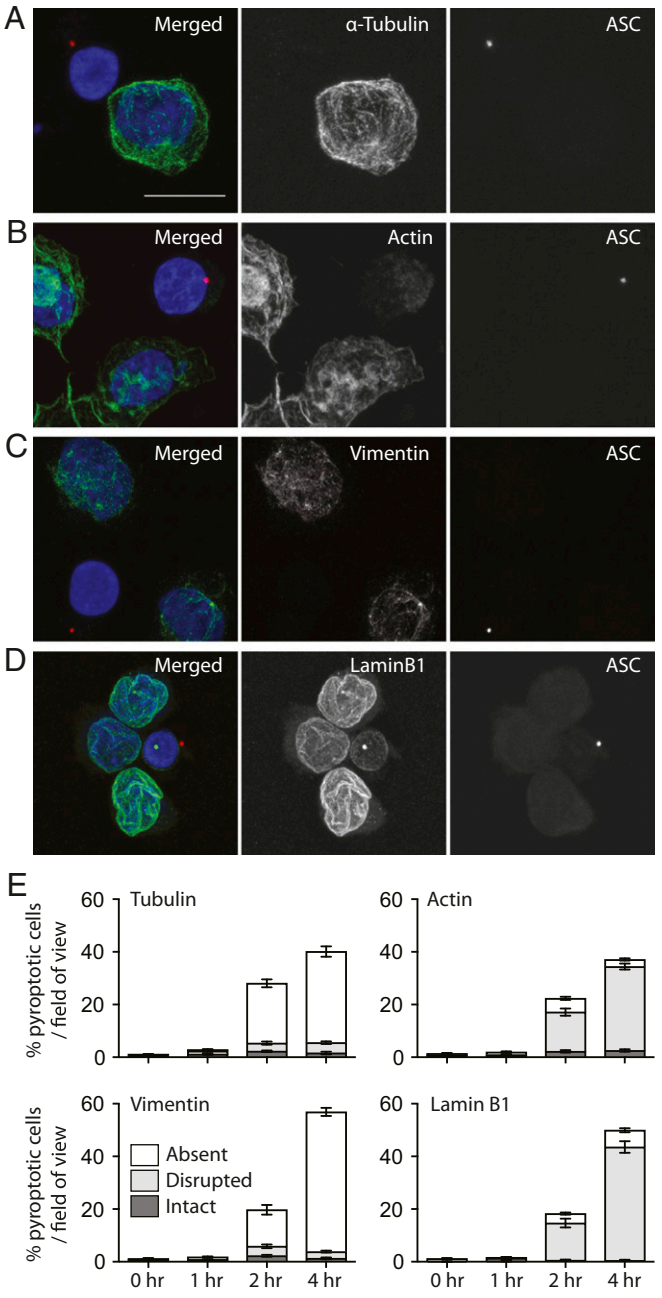

Fig. 3. The cytoskeleton is lost in pyroptotic THP-1 cells. (*A–D*) THP-1 cells were treated with Ng for 0, 1, 2, or 4 h to stimulate the NLRP3 inflammasome. Cells were fixed and stained for ASC (red) to mark the inflammasome, as well as DAPI to mark the nuclei. Cells were costained with α-Tubulin (*A*), actin (*B*), vimentin (*C*), or lamin B1 (*D*). (Scale bar: 10 μm.) (*E*) For quantitation of cytoskeletal loss, 5 to 10 random 40× fields-of-view at each time point were used to score cells for absent, disrupted, or intact cytoskeletal features. Error bars are SD.

S. typhimurium led to disruption of all cytoskeleton components in inflammasome-positive cells (Fig. 4*B*). These results demonstrate that activation of NLRP3 by LPS/Ng and NLRC4 activation by *Salmonella* leads to a loss of the entire cytoskeleton and that this effect occurs in primary cells from different species. Finally, to verify that cytoskeleton loss can occur in the absence of Casp1 and GSDMD, we assayed cytoskeleton loss in ΔCASP1 and in ΔGSDMD THP-1 cells. When treated with Ng, both ΔCASP1 and ΔGSDMD THP-1 cells underwent cytoskeleton catastrophe, although in delayed manner, as with cell swelling (*SI Appendix*, Fig. S4). Together, these data demonstrate that cytoskeleton loss is a fundamental pyroptotic event and suggest that cell swelling and cytoskeleton loss may be driven by a shared mechanism.

Calpain Drives Pyroptotic Cleavage of Vimentin and Loss of Intermediate Filaments. As with pyroptosis, microtubules, actin filaments, and intermediate filaments are also disrupted during apoptosis, wherein the mechanisms driving their disruption are linked to

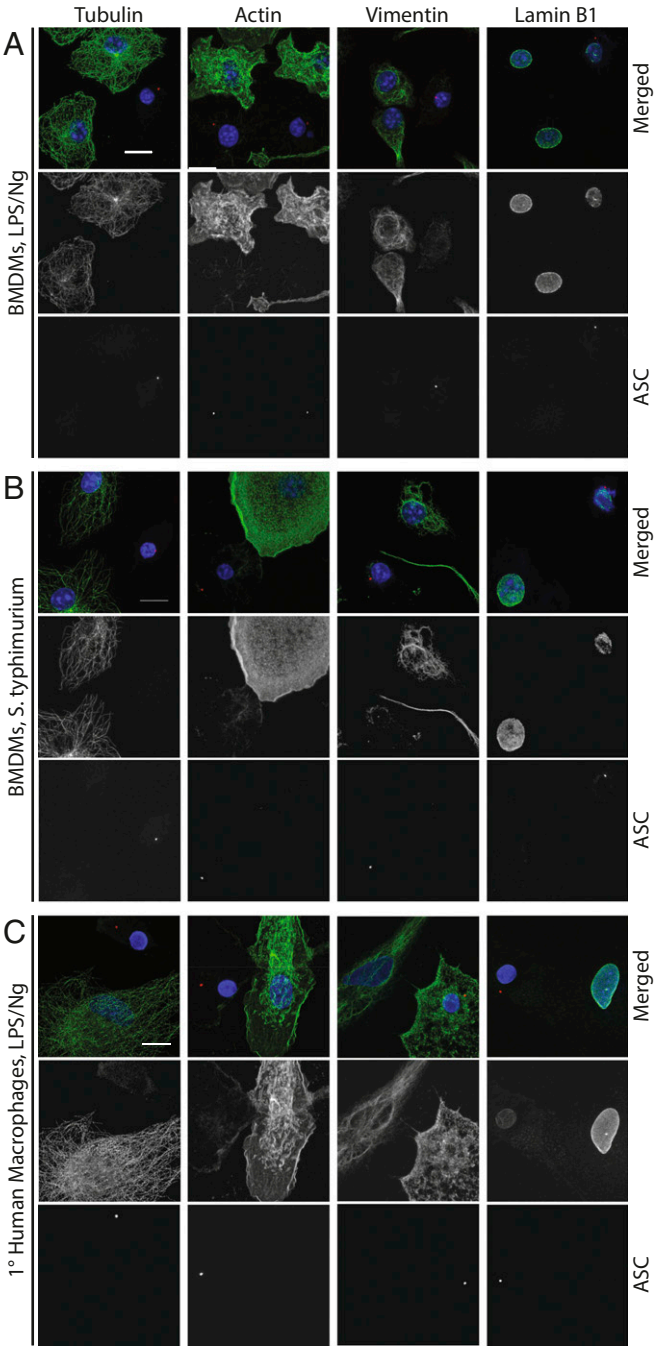

Fig. 4. Cytoskeleton loss is a general feature of pyroptosis. (*A*) BMDMs were treated with LPS/Ng to stimulate the NLRP3 inflammasomes. Cells were fixed and stained for ASC (red) to mark the inflammasome, as well as DAPI to mark the nuclei. Cells were costained for α-Tubulin, actin, vimentin, or lamin B1. (*B*) BMDMs were treated with *S. typhimurium* to activate the NLRC4 inflammasome and stained as in *A*. (*C*) 1° hMDMs were treated with LPS/Ng and stained as in *A*. (Scale bars for all panels: 10 μm.)

cleavage of tubulin, actin, and vimentin, among other cytoskeletal proteins (26–29). To determine whether similar cleavage occurs during pyroptosis, we stimulated THP-1 cells with Ng and evaluated the proteins present in cell lysates and supernatants by immunoblot assay (Fig. 5*A*). While cleaved IL-1β was present in supernatants of Ng-treated cells, we also observed the presence of cleaved vimentin, but not cleaved α-, β-, or γ-Tubulin or β-actin. These data suggest that vimentin cleavage may drive intermediate filament loss but that pyroptotic loss of microtubules or actin filaments is not linked to cleavage of tubulin or actin monomers.

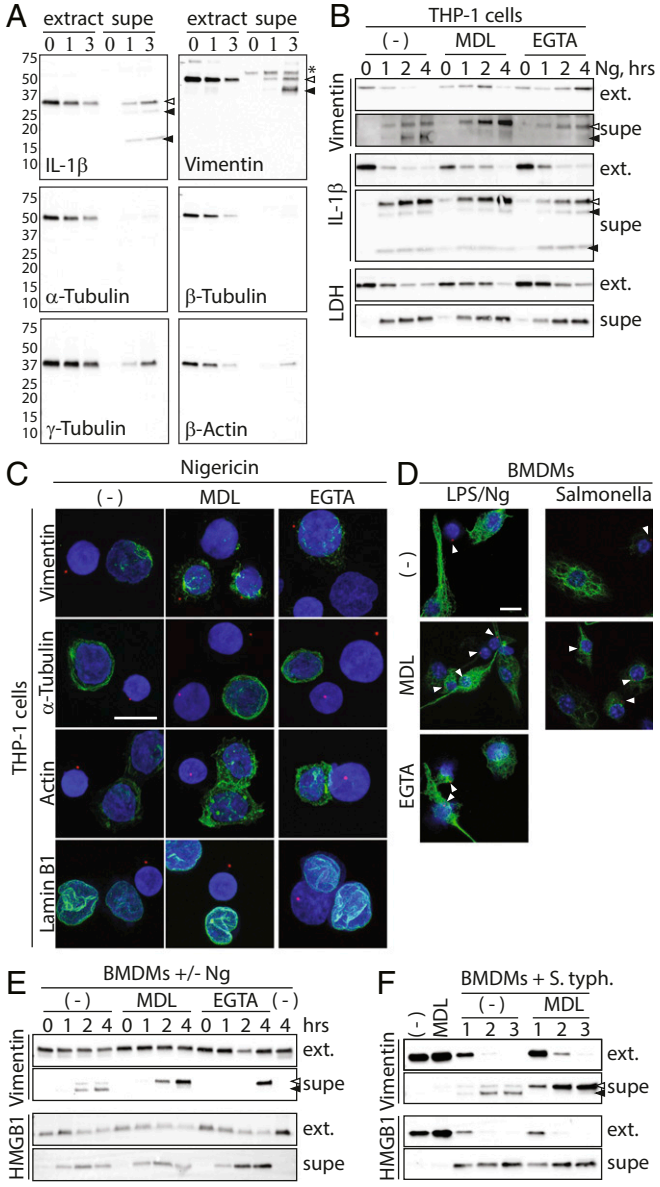

Fig. 5. Calcium and calpain drive pyroptotic cleavage of vimentin and loss of Intermediate filaments. (*A*) THP-1 cells were treated with Ng for 0, 1, or 3 h in serum-free medium. Extracts and supernatants were evaluated by immunoblot. Open and closed arrowheads indicate full-length and cleaved proteins, respectively. The asterisk indicates a nonspecific band. Numbers 75–10 indicate molecular weights and position of ladder bands. (*B*) THP-1 cells were treated for 0, 1, 2, or 4 h with Ng alone or with the calpain inhibitor MDL28170 or EGTA in serum-free medium. Cell extracts (ext.) and supernatants were evaluated by immunoblot. Arrowheads mark inflammasomes. (*C*) THP-1 cells were treated with Ng alone or with MDL28710 or EGTA. Cells were stained for ASC and with DAPI. Cells were costained for α-Tubulin, actin, lamin B1, or vimentin. Note that vimentin staining in inflammasome-positive cells is enhanced relative to non-pyroptotic cells. (Scale bar: 10 μm.) (*D*) BMDMs were treated with LPS/Ng and stained for intermediate filaments as in *C*. Arrowheads mark inflammasomes. (Scale bar: 10 μm.) (*E*) BMDMs were treated with LPS/Ng and evaluated as in *B*. (*F*) BMDMs were treated with *S. typhimurium* and evaluated as in *B*.

Microtubule and actin filaments are highly unstable (30, 31). Since tubulin and actin are not apparently cleaved during pyroptosis, loss of microtubules and actin may instead follow filament depolymerization. To determine if depolymerization drives pyroptotic cell swelling, we stabilized microtubules and actin filaments in THP-1 cells by treatment of cells with paclitaxel and/or jasplakinolide, respectively. Neither treatment alone or in combination prevented cell swelling (*SI Appendix*, Fig. S5*B*). Similarly, destabilization of microtubules and/or actin filaments with colchicine and/or cytochalasin D, respectively, was unable to drive cell swelling in nonpyroptotic cells (*SI Appendix*, Fig. S5*D*). Moreover, these pharmaceutical agents had no effect on Ng-induced cell death (*SI Appendix*, Fig. S5 *A* and *C*). Together these data argue against a role for microtubule and/or actin dynamics alone in pyroptotic cell swelling and instead suggest that cleavage of vimentin and loss of intermediate filaments are key features of pyroptotic cell swelling.

During apoptosis, vimentin is cleaved by the Ca^{2+}-dependent protease calpain (28). In fact, vimentin has six calpain cleavage sites in its amino terminus, cleavage at which results in apoptotic loss of intermediate filaments (32). To determine if calpain cleaves vimentin during pyroptosis, we treated THP-1 cells with Ng in the presence or absence of the calpain inhibitor MDL28170 or the calcium chelator EGTA. Both MDL28170 and EGTA prevented pyroptotic cleavage of vimentin, without inhibiting cleavage of IL-1β or the release of cleaved IL-1β or LDH from pyroptotic cells (Fig. 5*B*). Importantly, MDL28170 can inhibit cathepsin B, which is not calcium-dependent. Therefore, the fact that vimentin cleavage is similarly prevented by calcium chelation strongly indicates that pyroptotic vimentin cleavage is specifically dependent on calpain. Curiously, EGTA treatment increased full-length vimentin levels in cell extracts at 4 h; this observation was repeated several times. Furthermore, consistent with reports that Ng-induced inflammasome formation is independent of extracellular calcium (33) or calpain activity (34), neither EGTA nor MDL28170 prevented pyroptotic permeabilization or inflammasome formation (*SI Appendix*, Fig. S6). Importantly, we also observed a calpain-dependent cleavage of vimentin in BMDMs treated with LPS/Ng or infected with *S. typhimurium* (Fig. 5 *E* and *F*), demonstrating that vimentin cleavage is another fundamental pyroptotic event.

To determine whether Ca^{2+} and calpain are required for pyroptotic loss of intermediate filaments, we treated THP-1 cells with Ng in the presence or absence of MDL28170 or EGTA and visualized cytoskeletal structures (Fig. 5*C*). Importantly, as with vimentin cleavage, pyroptotic intermediate filament disruption was inhibited by both MDL28170 and EGTA. Moreover, intermediate filament staining in pyroptotic cells was seemingly enhanced upon MDL treatment relative to nonpyroptotic cells. Finally, neither calpain inhibition nor EGTA treatment prevented loss of actin filaments, microtubules, or nuclear lamina. These results were repeated in BMDMs treated with LPS/Ng or infected with *S. typhimurium* (Fig. 5*D*). Taken together, these observations indicate that Ca^{2+} and calpain-dependent cleavage of vimentin drives pyroptotic loss of intermediate filaments.

Pyroptotic Cells Lose Mechanical Resilience in a Calpain-Dependent Manner and Can Be Ruptured by Low Shear Stress and Compressive Force. Intermediate filaments generate a gel matrix within the cytosol that serves two general purposes: (*i*) They give the cell its elastic rigidity, allowing cells to be compressed and stretched without rupture, and (*ii*) they anchor cytosolic content, such as organelles, in 3D space (35). Thus, pyroptotic loss of intermediate filament gel matrix may make cells fragile and susceptible to

rupture by extrinsic forces found in vivo but not in vitro and may liquefy the cytosol to facilitate release of large cytosolic damage-associated molecular patterns (DAMPs), such as ASC specks, upon rupture. Of note, when we subjected cells to immunofluorescent staining, which causes significant fluidic shear stress with each change of solution, we often observed that pyroptotic cells are lost or ruptured, as indicted by the accumulation of cell-free inflammasomes. While some cell loss may result from destruction of actin and microtubules, calpain inhibition or EGTA treatment significantly increased the number of pyroptotic cells per field of view (Fig. 6 *A* and *B*). These observations are consistent with the outcome that pyroptotic rupture results from extrinsic forces, such as shear stress and intratissue compressive forces, and that rupture is blocked by calpain inhibition.

To directly determine if pyroptotic cells can be ruptured by fluidic shear stress, we subjected THP-1 cells to fluid flow in a flow cell chamber and imaged cells in real time by microscopy. Non-pyroptotic cells were able to withstand shear stresses of ~30 dynes/cm^2, without rupturing or even detaching from the plate. This shear stress is well within the range experienced in arteries (10 to 70 dynes/cm^2) (36). In contrast, Ng-treated, pyroptotic cells were largely blown off of the plate at shear stress as low as 1.5 dynes/cm^2 (Fig. 6*C*). This level of shear stress corresponds to the lowest stresses found in veins of the blood stream, which range from 1 to 6 dynes/cm^2 (36). Importantly, firmly attached pyroptotic cells were literally ripped apart as the shear stress distorted and stretched their plasma membranes until they ruptured, leaving behind an exposed nucleus (Fig. 6*D*, *SI Appendix*, Fig. S7, and Movie S5). Calpain inhibition blocked detachment of pyroptotic cells at low fluidic shear stress but not at higher fluidic shear stress (>10 dynes/cm^2). These data suggest that detachment may be regulated by intermediate filament loss at low shear stress and by loss of actin filaments and microtubules at high shear stress as actin filaments and microtubules were unaffected by calpain inhibition and the fact that microtubules and actin filaments play critical roles in cell adhesion. Importantly, no attached cells were observed to rupture upon calpain inhibition. These data demonstrate that pyroptotic cells are sensitive to rupture and detachment at the lowest shear forces experienced in vivo and that shear force-dependent sensitivity to rupture is mediated by the proteolytic activity of calpain.

Cell–cell attachments create nanonewton (nN) intratissue compressive forces (37). To evaluate the sensitivity of pyroptotic cells to these compressive forces, we used atomic force microscopy (AFM) to apply nN forces to cells in culture and measured their resistance to compression (*SI Appendix*, Fig. S8). Furthermore, if a cell bursts, this technique registers the resulting loss of resistance and detects the force at which resistance was lost (*SI Appendix*, Fig. S8, *Lower*). In this manner, Ng-treated and untreated THP-1 cells were subjected to an increasing force up to 15 nN. Remarkably, 77% of Ng-treated cells burst (Fig. 6*E*) while untreated cells never ruptured. Moreover, calpain inhibition largely prevented the compressive rupture of Ng-treated cells by AFM. Importantly, pyroptotic cells ruptured at an average force of only 6.6 nN or about 0.02 nN/μm^2, which is 170-fold lower than the tissue stresses measured by Campàs et al. (37). These observations demonstrate that intratissue forces found in vivo can rupture pyroptotic cells and that this process occurs in a calpain-dependent manner.

In addition to providing mechanical resilience, the intermediate filament gel matrix also cages organelles and cytoplasmic structures within three-dimensional space, preventing free movement throughout the cytosol (28). We found that mCherry-tagged inflammasomes move freely throughout the cytoplasm of roughly 70% of pyroptotic cells in a manner suggestive of random Brownian motion and liquefaction of the cytosol following intermediate filament loss (Figs. 2*E* and 6*F* and Movie S4). Importantly, ASC-speck mobility within pyroptotic cells was largely prevented when calpain was inhibited with MDL28170 (Fig. 6*F* and Movie S6). Thus, pyroptotic, calpain-dependent cytosol liquefaction facilitates release of ASC specks and possibly other large cytoplasmic structures upon rupture.

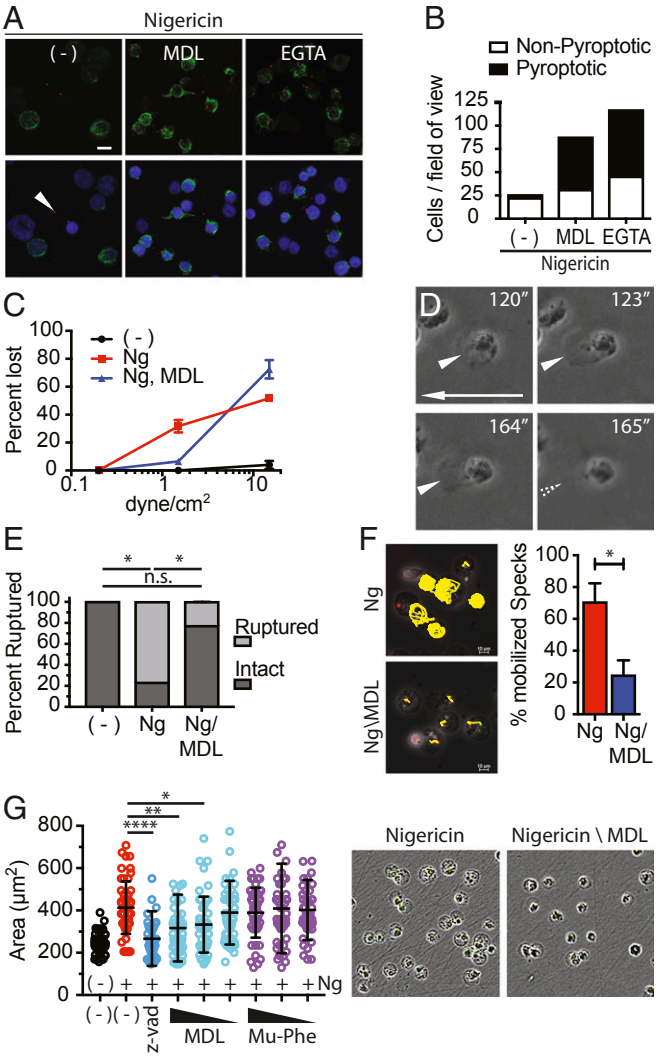

Fig. 6. Calpain drives pyroptotic fragility, cytosolic liquefaction, and cell swelling. (*A*) THP-1 cells were treated with Ng alone or with MDL28170 or EGTA. Cells were fixed and stained for ASC and vimentin. The arrowhead marks a cell-free inflammasome. (*B*) Quantitation of *A*. Five random 40× fields-of-view were quantified. The graph is representative of multiple experiments. (*C*) THP-1 cells were untreated or treated with Ng alone or with MDL28170 for 2 h. Cells were subjected to fluidic shear stress and imaged over time. Images were analyzed, and cell detachment was quantified as a function of shear stress. (*D*) THP-1 cells were treated as in *C* and subjected to a shear stress of 1.5 dynes/cm^2. Images show seconds after start of flow, and the arrow shows direction of flow. Arrowheads point to cells distorted and ruptured by shear stress (Movie S5). (*E*) THP-1 cells were untreated or treated with Ng ± MDL28170 and subjected to 15 nN of compressive force by atomic force microscopy (AFM). The percentage of cells ruptured under each condition was quantified. *P* values were calculated with Student's *t* test. **P* < 0.5; n.s., nonspecific. (*F*) THP-1 cells expressing ASC-mCherry were treated with Ng ± the MDL28170 and imaged. Inflammasomes were tracked in 2D using the TrackMate plugin of ImageJ/FIJI. The percentage of cells with mobile inflammasomes was quantified. Error bars are SD. Significance calculated with unpaired *t* test; **P* < 0.5. (*G*) THP-1 cells were treated with Ng ± Z-VAD or decreasing concentrations of MDL28170 or the cathepsin B inhibitor Mu-Phe-hPhe-FMK and imaged via IncuCyte analysis. Cell swelling was quantified from IncuCyte images using ImageJ/FIJI. Error bars are SD. Representative images are merged phase and green channel images of cells treated with Ng ± MDL28170. Significance calculated via one-way ANOVA using Dunnett's multiple comparison test. *****P* = 0.0001, ***P* < 0.005, **P* < 0.05.

To assess the role of calpain in cell swelling, we treated THP-1 cells with Sytox alone or with Ng in the presence or absence of decreasing concentration of MDL28170 and followed the cells by IncuCyte analysis (Fig. 6*G*). As controls, we also treated cells with the pan caspase inhibitor Z-VAD (which also inhibits calpain) or the cathepsin B inhibitor Mu-Phe-hPhe-FMK. Cotreatment of cells with Ng and Z-VAD prevented cell swelling and permeabilization (Fig. 6*G*), as determined by Sytox uptake. This outcome is consistent with the role of Casp1 in cleaving GSDMD and driving GSDMD pore formation that results in cell permeabilization. Conversely, calpain inhibition prevented Ng-induced cell swelling in a dose-dependent manner although cells were still permeabilized and therefore still open to calcium and water. Cathepsin B inhibition had no effect on the cell. Together, these data show that pyroptotic cell swelling is an active process driven by calcium flux and calpain activation.

Rupture of Pyroptotic Cells Releases Macro-DAMPs and Is Immunostimulatory. Our data demonstrate that pyroptotic cells do not rupture in vitro but can be ruptured by forces found in vivo, suggesting that rupture may release macromolecules that are not released by diffusion alone. To determine if pyroptotic rupture indeed releases ASC specks, THP-1 cells expressing mCherry-tagged ASC were subjected to fluidic shear stress in a fluid cell chamber and visualized in real time. Before increasing flow rate, ASC specks were readily discernible in pyroptotic cells. Additionally, as with WT THP-1 cells, most cells detached as a result of increasing shear stress. Importantly, we were able to visualize release of ASC specks from pyroptotic cells ruptured by shear stress (Fig. 7*A* and Movie S7), demonstrating that rupture of pyroptotic cells could release these immunostimulatory bodies.

We also assessed the release of other large cytosolic inflammatory content from pyroptotic cells upon rupture. Of note, immunostimulatory mitochondria are reportedly released from necroptotic and neutrophil extracellular trap (NET) forming cells (38, 39), and our data suggest that they should also be released by pyroptotic rupture. Therefore, we subjected pyroptotic THP-1 cells to shear stress by pipetting to rupture the cells. Culture supernatants were carefully removed to prevent disruption of unruptured cells and gently centrifuged at 300 × *g* to pellet large debris and unruptured cells. Cleared supernatants were then separated from pelleted material. In this manner we generated three fractions from each sample: (*i*) cell extracts, (*ii*) low speed pellets from culture supernatants, and (*iii*) cleared supernatants. It is important to note that, while 300 × *g* seems to be a relatively large force, force is calculated as mass times acceleration, and the mass of a cell (10^{-12} kg) in liquid is quite small. As a result, 300 × *g* exerts less force than the rupture point calculated by AFM by an order of magnitude. It is also important to note that shear stress exerted by pipetting was enough to detach some untreated nonpyroptotic cells; however, these cells remained intact and viable, as evidenced by their morphology and their unpermeabilized membranes (Fig. 7*C*). All fractions were first evaluated by immunoblot analysis for protein content and by qPCR for mitochondrial and nuclear DNA. We found that the presence of IL-1β and LDH in cleared supernatants was unaffected by pyroptotic rupture (Fig. 7*B*), consistent with their diffusion through the GSDMD pores. However, levels of mitochondrial DNA and the mitochondrial protein CoxI were greatly increased in cleared supernatants from ruptured pyroptotic cells. These observations were recapitulated in BMDMs (Fig. 7*D*). Similarly, lysosomes, as detected by Lamp1, were only detected in the cleared supernatants of ruptured pyroptotic cells (Fig. 7*B*), but not in cleared supernatants from nonruptured pyroptotic cells. Finally, microscopy-based analysis of low speed pellets from culture supernatants revealed the presence of numerous cell-free, naked nuclei from ruptured samples (Fig. 7*C*). In contrast, low speed (300 × *g*) pellets from supernatants of nonruptured, pyroptotic cells predominantly contained swollen yet intact cells and very few naked nuclei, which were likely generated as samples were processed for analysis. Together, these data suggest that all cytosolic content is likely exposed upon pyroptotic rupture.

Pyroptotic cells infected with *Salmonella* have been shown to form traps that contain immobile bacteria and prevent bacteria release (40). These conclusions were based in large part on live-cell imaging of cells that were not subjected to extrinsic forces and therefore not ruptured. To determine if *Salmonella*-infected cells would rupture and release bacteria, we infected BMDMs with GFP-expressing *S. typhimurium* and imaged them in our flow cell chamber. As reported, and in contrast to our observations of highly mobile intracellular ASC specks, intracellular bacteria were indeed rather immobile. Importantly, as with WT THP-1 cells, infection of BMDMs with GFP-*Salmonella* resulted in fragile cells that were ruptured at 1.5 dynes/cm^2 (Fig. 7*E*). Also, because BMDMs are inherently more adhesive than THP-1 cells, there were many more rupture events than with THP-1 cells and many fewer cells that simply detached from the culture dish. However, while we were able to identify some bacteria released by rupture, most bacteria remained encased within pyroptotic bodies torn off of the main cell mass or with the ruptured cell corpses (Fig. 7*E*), thus supporting the observations of Jorgensen et al. (40).

Finally, to determine whether rupture enhances the inflammatory response to pyroptosis, we fractionated Ng-treated, pyroptotic THP-1 cells as above and used the cleared supernatants and supernatant pellets to stimulate primary neutrophils for 1 h ex vivo. After treatment, neutrophils were analyzed by flow cytometry for classic markers of activation: CD11b, CD66b, and CD63 (Fig. 7*F*). Given that nonruptured pyroptotic cells release IL-1β and HMGB1, cleared supernatants from nonruptured pyroptotic THP-1 cells activated neutrophils and increased the abundance of all three markers to a small degree. In contrast, the levels of all these markers were strikingly and significantly increased when neutrophils were treated with cleared supernatants from ruptured pyroptotic cells. Together, these data demonstrate that products of pyroptotic cell rupture enhance neutrophil activation and thus the inflammatory response.

Discussion

Our observations advance the mechanistic understanding of cellular events that occur during pyroptosis, as well as their inflammatory consequences, and they clarify mechanisms (diffusion and rupture) by which cytosolic material is released upon pyroptotic cell death. Specifically, we show that pyroptotic cells swell in vitro but do not rupture. We discovered that loss of the entire cytoskeleton—microtubules, actin filaments and intermediate filaments, and nuclear lamina—is a fundamental feature of pyroptosis. We also demonstrate that the Ca^{2+}-dependent protease calpain drives cleavage of vimentin and dissolution of the intermediate filaments, as well as pyroptotic cell swelling. Our data are consistent with a model (*SI Appendix*, Fig. S9) whereby GSDMD-mediated permeabilization of the plasma membrane permits a massive influx of Ca^{2+} to activate calpain and drive many of the observed responses; both GSDMD-mediated Ca^{2+} influx and pyroptotic calpain activation have been reported previously (41, 42). Interestingly, we show that inflammasome-dependent cell swelling occurred in Casp1 and GSDMD knockout THP-1 cells in the absence of cell permeabilization and was sensitive to Z-VAD, a pan caspase and calpain inhibitor. Whether swelling in these cells was dependent on calpain is unclear, as is the presumed source of calcium, which could possibly be mobilized from intracellular stores and/or from external sources. Importantly, pyroptotic intermediate filament loss correlates with a dramatic loss of mechanical resilience and liquefaction of the cytoplasm, both of which are prevented by calpain inhibition. As a result, pyroptotic cells become extremely fragile and can rupture if subjected to shear stress or compressive forces smaller than those found in vivo. Moreover, rupture is not required for release of classic markers of pyroptosis, such as LDH, IL1-β, and HMGB1, suggesting that these markers are released by passive diffusion

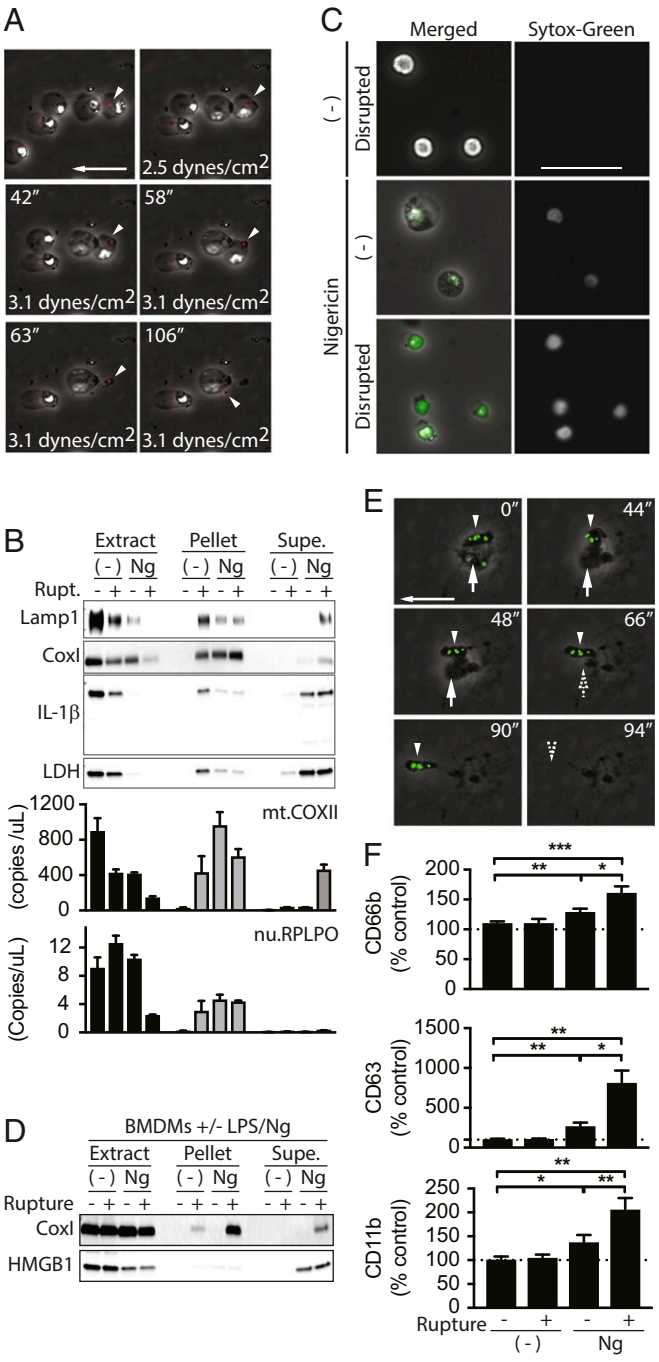

Fig. 7. Rupture of pyroptotic cells releases and exposes nondiffusible cytosolic content and enhances immunostimulation. (*A*) ASC.mCherry expressing THP-1 cells were treated with Ng for 2 h and then subjected to shear stress and imaged. Rupture of attached, inflammasome-positive cells is shown. Arrow shows direction of flow and is 50 μm. Arrowheads track inflammasome release upon rupture (Movie S7). (*B*) THP-1 cells were treated with Ng or not for 4 h. Cells were ruptured or not by mechanical disruption. Supernatants were carefully removed and cleared by low speed centrifugation. Cleared supernatants, the remaining pellet, and cell extracts were analyzed by immunoblot with normalized volumes or by qPCR for mitochondrial (mt.COXII) or nuclear (nu.RPLPO) DNA. (*C*) THP-1 cells were treated as in *B*. Low speed centrifugation pellets from supernatants were treated with Sytox and imaged. (Scale bar: 50 μm.) (*D*) BMDMs were treated and analyzed as in *B*. (*E*) BMDMs were treated with GFP-expressing *S. typhimurium* and subjected to 1.5 dynes/cm^2 as in *A*. Rupture of salmonella-containing cells was tracked over time. Arrowhead points to bacteria that stay within ruptured pyroptotic body. Vertical arrow points to bacterium that is released from ruptured cell. Horizontal arrow shows direction of flow and serves as scale bar (50 μm). (*F*) THP-1 cells were treated as in *B*. Cleared supernatants and supernatant pellets were used to treat primary neutrophils ex vivo. Activation of neutrophils was assayed by flow cytometry. Significance calculated with paired *t* test. *$P < 0.5$, **$P < 0.01$, ***$P < 0.001$.

through GSDMD pores. Furthermore, rupture releases larger nondiffusible cytosolic content that enhances immunostimulation. Together, these observations reveal unappreciated cellular events that occur during pyroptosis, they define a mechanism by which pyroptotic cells rupture, and they reveal the immune-stimulatory outcome of cell rupture to activate neutrophils. It would be worthwhile to conduct studies to define how and which cytosolic constituents directly contribute to immunologic responses from pyroptosis.

Cytoskeleton Disruption. We show that actin filaments, microtubules, intermediate filaments, and nuclear lamina are disrupted as a general feature of pyroptosis. These observations are consistent with studies by Salinas et al. (43) demonstrating that microtubules are lost following *Salmonella* infection of BMDMs. The role of actin filaments and microtubule disruption during pyroptosis is still unclear. However, pyroptotic intestinal epithelial cells are physically excluded from the gut epithelium monolayer (11), and, as the cortical actin cytoskeleton plays a large role in maintaining cell–cell contacts and the integrity of epithelial monolayers, loss of actin filaments may facilitate and even force the exclusion of these cells into the lumen of the intestines.

Our observations are consistent with a model where calpain cleaves vimentin to disrupt intermediate filaments and drive cell fragility. We note that some of our results are based on the use of the calpain I/II inhibitor MDL28170, which has broader specificity to also inhibit cathepsin B, thus raising a possibility of off-target effects. However, as calpain, but not cathepsin B, is calcium-dependent, we typically compared the effects of MDL28170 with those of EGTA to demonstrate that observed effects were specifically dependent on calpain. Moreover, vimentin is among ∼70 intermediate filament family members (35). Thus, beyond vimentin, it is likely that other intermediate filament proteins are also cleaved during the process of pyroptotic cell rupture. Finally, we note that vimentin was shown to bind NLRP3 and regulate its activation (44), but our observations of vimentin cleavage describe events downstream of inflammasome activation. The relationship of the NLRPR3–vimentin interaction and pyroptotic cleavage of vimentin remains to be determined.

Immunologic Consequences of Pyroptotic Rupture. Our data suggest that soluble proteins as large as 200 kDa (microDAMPs) are able to transit through the GSDMD pore by passive diffusion but that large and/or nonsoluble content (macroDAMPs) require rupture for release. Most studies have focused on the downstream immune responses to IL-1β, IL-18, HMGB1, and ATP. Importantly, however, our data suggest that the full immunostimulatory potential of pyroptosis is only achieved upon cell rupture. There are a number of likely inflammatory candidates released as pyroptotic cells burst, including ASC specks (5), mitochondria (38), and mitochondrial DNA (39). We also show that nuclei are exposed to the extracellular milieu upon rupture. As pyroptotic release of DNA is thought to result in anti-nuclear antibodies that drive pathology in systemic lupus erythematosus (SLE) (6), it is possible that the release of nuclei from pyroptotic cell rupture mechanistically underscores the onset of anti-nuclear antibodies in SLE development to exposed nuclei. This possibility is supported by studies of the murine model of SLE in which Casp1 knockout inhibited production of anti-nuclear antibodies (45).

Stimulation of pyroptosis following infection by intracellular pathogens has long been assumed to result in a destruction of a replicative niche. This could occur through one or two mechanisms, neither of which is mutually exclusive. First, permeabilization of the plasma membrane should permit egress of ATP and building blocks

necessary for pathogen replication. Second, rupture should release pathogen replication intermediates to potentially aid in stimulation of the downstream inflammatory response. Moreover, Jorgensen et al. (40) demonstrated that *Salmonella* recovered from pyroptotic cells were less viable, indicating that pyroptosis could also render intracellular pathogens inert and then use them to aid in propagating the downstream inflammatory response. This outcome would apparently be to the detriment of the pathogen as a population. However, Jorgensen et al. (40) also demonstrated that intracellular *Salmonella* are immobilized within pyroptotic BMDMs in a manner that was not dependent on actin or microtubules. They further showed that BMDMs in vitro and neutrophils in vivo could phagocytize pyroptotic macrophages bearing GFP-expressing *Salmonella*. These results support an outcome in which *Salmonella* are trapped within pyroptotic cells for clearance by phagocytes. Our data are consistent with this model, even in the face of apparent rupture of the *Salmonella*-infected cells, as we demonstrate that *Salmonella* are trapped within pyroptotic bodies torn off BMDMs following rupture. Interestingly, this is in stark contrast to our results in Ng-treated THP-1 cells where rupture-released ASC specks, mitochondria, and nuclei were free and not encased in cellular debris. Why *Salmonella* in BMDMs behave differently than ASC specks and nuclei in THP-1 cells is currently unclear, but these differences could reflect the properties of the bacterial intracellular life cycle.

Summary. Our study identifies previously unrecognized events occurring during pyroptosis. These include calpain-dependent cleavage of vimentin, loss of intermediate filaments, liquefaction of the cytosol, and loss of mechanical resilience, as well as loss and disruption of microtubules, actin filaments, and nuclear lamina. We demonstrate that pyroptotic cells are ruptured by mechanical force and that rupture is blocked by calpain inhibition. Moreover, we show that rupture is immunostimulatory and releases ASC specks, mitochondria, mitochondrial DNA, nuclei, and bacteria. Our data support a mechanism of pyroptotic rupture where GSDMD pores permit a calcium influx that activates calpain. As such, pyroptotic rupture may be susceptible to pharmaceutical intervention that may lessen the severity of chronic inflammation caused by pathogens, autoimmune diseases, and cancer.

Methods

Cell Culture. Bone marrow-derived macrophages (BMDMs) were generated as described previously (46). BMDMs and THP-1 cells [TIB-202; American Type Culture Collection (ATCC)] were grown in RPMI supplemented with 10% heat-inactivated FBS, 1% antibiotic/antimycotic, 1% L-glutamine, 1% nonessential amino acids, and 1% sodium pyruvate. For experiments, THP-1 cells were differentiated with 40 nM phorbol myristate acetate (PMA) for 16 to 20 h and rinsed with PBS before use. Human peripheral blood mononuclear cells (PBMCs) were isolated from the blood of healthy donors using a Ficoll Paque Plus (GE Healthcare) density gradient. Monocytes were roughly purified by their inability to adhere to noncoated plates over 1 to 3 h at 37 °C. Nonadherent PBMCs were then collected and cultured for 7 d in complete RPMI supplemented with macrophage-colony stimulating factor (Peprotech). Collection and use of primary human PBMCs followed informed consent and was approved by the University of Washington Institutional Review Board (study 00003100).

Inflammasome Activation. To activate the NLRP3 inflammasome, PMA-differentiated THP-1 cells were stimulated with 10 μM Ng. BMDMs and primary human monocyte-derived macrophages were treated with 5 ng/mL or 50 ng/mL LPS (from *Salmonella abortus*), respectively, for 4 h, and then treated with 10 μM Ng. To activate the AIM2 inflammasome, PMA-differentiated THP-1 cells or BMDMs were transfected with 1 μg/mL calf thymus DNA using the Mirus TransIT-LT1 transfection reagent.

CRISPR. CRISPR gRNA sequences were selected using https://zlab.bio/guide-design-resources. Typically, four independent gRNAs were selected per gene. gRNA sequences were subcloned into the pRRL-empty-gRNA-Cas9-T2A-Puro vector (47) via InFusion cloning (TaKaRa). Constructs were transduced into THP-1 cells by spin-fection, and polyclonal populations were isolated by puromycin selection. Puromycin-resistant cells were then screened by western analysis, as well as by IncuCyte-based cell death analysis to verify that the gene of interest was sufficiently knocked out. ASC gRNA sequences were as follows: gRNA16 (GCTGGAGAACCTGACCGCCG) and gRNA21 (GAACTTCTTGAGCTCCTCGG). CASP1 gRNA sequences were as follows: gRNA1 (AAGCTGTTTATCCGTTCCAT) and gRNA4 (TTTATCCGTTCCATGGGTGA). GSDMD gRNA sequences were as follows: gRNA2 (CGGCCTTTGAGCGGGTAGTC), gRNA13 (GGTAGTCCGGAGAGTGGTCC), gRNA19 (AGCCCTACTGCCTGGTGGTT), and gRNA 24 (CAGGGATGAACTCCCCACCA). NLRP3 gRNA sequences were as follows: gRNA1 (TCTCTGTCTGACCCCTCGGG) and gRNA3 (CTGCAAGCTGGCCAGGTACC). The nonsilencing control (NSC) gRNA sequence was as follows: ACGGAGGCTAAGCGTCGCAA (48).

IncuCyte Zoom Live-Cell Imaging. PMA-differentiated THP-1 cells were seeded on 24-well dishes at either 400,000 or 100,000 cells per well. Cells were treated with 100 nM Sytox (Sytox) (S7020; Thermo Fischer) to assay cell death and/or permeabilization or in separate wells with Syto-Green (S7559; Thermo Fischer) to assay total cell number. Cells were imaged with the IncuCyte imaging platform (Essen Bioscience). At each time point, four images were taken per well. Each treatment was run in either duplicate or triplicate. Percent cell death was calculated by averaging Syto-Green counts over 2 h near the beginning of the run. These were averaged with replicates and used to normalize Sytox counts to calculate percent cell death. For quantitation of cell swelling, IncuCyte images were imported into ImageJ/FIJI, and area measurements were made on >50 cells from a single field of view for each condition.

Immunofluorescence. Cells were plated on glass coverslips and treated as indicated. At indicated time points, cells were fixed with 3% paraformaldehyde for 30 min at room temperature. Cells were washed twice with PBS/glycine, permeabilized with 0.2% Triton X-100 in PBS, and then washed again with PBS/glycine. Nonspecific binding was blocked with 3% milk in PBS for ∼10 min at room temperature. Primary antibodies were diluted in 3% milk and incubated for 30 min at room temperature while rocking. Cells were then washed briefly three times in PBS. Secondary antibodies and DAPI were diluted in 3% milk and incubated for 30 min at room temperature while rocking in the dark. Cells were then washed briefly three times in PBS. Coverslips were dipped in 100% EtOH and air dried before mounting with Prolong Gold Antifade Reagent (P36934; Life Technologies). Antibodies were as follows: ASC (sc-22514, 1:10,000; Santa Cruz) (D086-3, 1:600; MBL), α-Tubulin (DM1A, T6199, 1:2,000; Sigma), β-Tubulin (BAB8527, 1:100; R&D Systems), pericentrin (ab28144, 1:300; Abcam), Phalloidin-488 (A12379, 1:600; Life Technologies), vimentin (V6630, 1:500; Sigma), lamin B1 (ab16048, 1:600; Abcam), goat anti-mouse IgG1 (A21125, 1:600; Invitrogen), goat anti-rabbit IgG (A32733, 1:600; Invitrogen), and goat anti-mouse IgG2b (A21242, 1:600; Invitrogen).

Immunoblot Analysis. For conditions where supernatants would be analyzed, cells were typically treated with serum-free medium. Cells were lysed with Nonidet P-40 lysis buffer containing EDTA (1 mM), PMSF (1 mM), okadaic acid (250 μM), protease inhibitor mixture (P3340; Sigma), and phosphatase inhibitor mixture (524625; Calbiochem). Antibodies were as follows: α-Tubulin (T6199; Sigma) (2144; Cell Signaling Technology); acetylated-α-Tubulin (ab11323; Abcam); β-Tubulin (BAB8527; R&D Systems); γ-Tubulin (T5326; Sigma); β-actin (sc-4778; Santa Cruz); NLRP3 (AG-20B-0014; Adipogen); ASC (D086-3; MBL); Casp1 (sc-515; Santa Cruz) (4199S; Cell Signaling Technology); and GSDMD (sc-81868; Santa Cruz).

Fluid Flow Experiments. Cells were cultured as described above and incubated overnight on a Corning brand polystyrene tissue culture dish at 37 °C. Cells were then washed with PBS and untreated or treated with Ng with or without MDL28170. Cells were mounted into a Glycotech parallel plate flow chamber (Glycotech) and washed with PBS plus 0.2% BSA at room temperature using a syringe pump with a stepwise increase in flow rate, to apply the indicated levels of shear stress for 30 s each. Cells were monitored with digital video microscopy at 1 frame per second, and the fraction of cells that were originally present at 0.2 dyne/cm^2 was calculated at the end of the 30 s at each shear stress. The average and SD were calculated for four videos in each condition.

Atomic Force Microscopy. Cells were prepared as described above. Cells were placed on an Asylum MFP-3D AFM, with integrated top-down optics. Tipless cantilevers (Pnp-TR-TL_Au; NanoWorld) were blocked overnight in PBS-BSA, and the spring constant was measured with the thermal method (between 28 and 36 pN/nm). Individual cells were located visually and compressed with the cantilever at a constant velocity of 0.5 μm/s until a 15-nN compressive force was reached, at which point the tip was withdrawn. When a cell

ruptured, the force suddenly dropped, and the rupture force was measured as the difference between the peak of compressive force and the force following the drop in force. The experiments were repeated on two different days on which the conditions were tested in a different order. The average and SD of each measurement was calculated for the 2 d, and *P* values were determined using Student's two-tailed paired *t* test.

Neutrophil Activation. Human neutrophils were isolated using Polymorphprep as described previously (39, 49, 50). For activation, neutrophils (1×10^6 cells per mL) were incubated with pyroptotic supernatant (20%) for 90 min before assessment of neutrophil activation markers CD11b, CD66b, and CD63 (BioLegend) using flow cytometry (CytoFlex; Beckman Coulter). Data were analyzed by FlowJo (Tree Star, Inc.).

DNA Extraction and Real-Time Quantitative PCR. DNA was isolated from supernatants, pellets, and lysed cell suspensions using a Plasma/Serum Cell-Free Circulating DNA Purification Micro Kit following the manufacturer's instructions. The StepOnePlus Real-Time PCR System was used to perform quantitative PCR. Primer sequences for nuclear (ribosomal protein lateral stalk subunit P0, RPLP0) (51) and mitochondrial gene (cytochrome *c* oxidase subunit II, Cox II) (52) targets have been reported previously. Further, specificity of mitochondrial primers was confirmed by screening through BLAST and University of California, Santa Cruz (UCSC) genome browser databases, to ensure that primers did not coamplify nuclear embedded mitochondrial DNA sequences. PCR was set up in a volume of 20 μL containing 1× Power SYBR Green PCR Master Mix, one pair of primers directed against nuclear or mitochondrial genes at a final concentration of 100 nM, 5 μL of isolated DNA, and 3 μL of PCR-grade water. Each PCR was performed as follows: incubation for 2 min at 50 °C, followed by a first denaturation step of 10 min at 95 °C and 40 cycles of 95 °C for 15 s, 55 °C (COXII) or 60 °C (RPLP0) for 1 min; and 60 °C for 1 min. Absolute quantification of gene targets was derived from a standard curve created by serial dilutions of synthesized nuclear and mitochondrial genes. In each run, nontemplate negative controls were also included. Postamplification melting curve analysis was performed to confirm the specificity of the amplification.

ACKNOWLEDGMENTS. We thank Andrey Suvarikov, Lauren Aarreberg, and Amina Negash for feedback throughout the project. We thank Elizabeth Grey and Dan Stetson for the nonsilencing gRNA and the lentiviral backbone used to generate the other CRISPR constructs. This work was supported by NIH Grants AI127463, AI118916, AI100625, AI108319, AI104002, T32 AI106667, AI106987, and K08 AI119142 as well as NSF Grant CMMI-1824792 and funding from Lupus Research Alliance (Grant 519414).

1. Mathur A, Hayward JA, Man SM (2018) Molecular mechanisms of inflammasome signaling. *J Leukoc Biol* 103:233–257.
2. Kovacs SB, Miao EA (2017) Gasdermins: Effectors of pyroptosis. *Trends Cell Biol* 27: 673–684.
3. Fink SL, Cookson BT (2006) Caspase-1-dependent pore formation during pyroptosis leads to osmotic lysis of infected host macrophages. *Cell Microbiol* 8:1812–1825.
4. den Hartigh AB, Fink SL (2018) Pyroptosis induction and detection. *Curr Protoc Immunol* 122:e52.
5. Franklin BS, et al. (2014) The adaptor ASC has extracellular and 'prionoid' activities that propagate inflammation. *Nat Immunol* 15:727–737.
6. Magna M, Pisetsky DS (2015) The role of cell death in the pathogenesis of SLE: Is pyroptosis the missing link? *Scand J Immunol* 82:218–224.
7. Sborgi L, et al. (2016) GSDMD membrane pore formation constitutes the mechanism of pyroptotic cell death. *EMBO J* 35:1766–1778.
8. Mulvihill E, et al. (2018) Mechanism of membrane pore formation by human gasdermin-D. *EMBO J,* 37:e98321.
9. He WT, et al. (2015) Gasdermin D is an executor of pyroptosis and required for interleukin-1β secretion. *Cell Res* 25:1285–1298.
10. Mascarenhas DPA, et al. (2017) Inhibition of caspase-1 or gasdermin-D enable caspase-8 activation in the Naip5/NLRC4/ASC inflammasome. *PLoS Pathog* 13:e1006502.
11. Rauch I, et al. (2017) NAIP-NLRC4 inflammasomes coordinate intestinal epithelial cell expulsion with eicosanoid and IL-18 release via activation of caspase-1 and -8. *Immunity* 46:649–659.
12. Schneider KS, et al. (2017) The inflammasome drives GSDMD-independent secondary pyroptosis and IL-1 release in the absence of caspase-1 protease activity. *Cell Rep* 21: 3846–3859.
13. Wang Y, et al. (2017) Chemotherapy drugs induce pyroptosis through caspase-3 cleavage of a gasdermin. *Nature* 547:99–103.
14. de Vasconcelos NM, Van Opdenbosch N, Van Gorp H, Parthoens E, Lamkanfi M (2018) Single-cell analysis of pyroptosis dynamics reveals conserved GSDMD-mediated subcellular events that precede plasma membrane rupture. *Cell Death Differ* 26:146–161.
15. Feng S, Fox D, Man SM (2018) Mechanisms of gasdermin family members in inflammasome signaling and cell death. *J Mol Biol* 430:3068–3080.
16. Man SM, Karki R, Kanneganti TD (2017) Molecular mechanisms and functions of pyroptosis, inflammatory caspases and inflammasomes in infectious diseases. *Immunol Rev* 277:61–75.
17. Wallach D, Kang TB, Dillon CP, Green DR (2016) Programmed necrosis in inflammation: Toward identification of the effector molecules. *Science* 352:aaf2154.
18. Shi J, et al. (2015) Cleavage of GSDMD by inflammatory caspases determines pyroptotic cell death. *Nature* 526:660–665.
19. DiPeso L, Ji DX, Vance RE, Price JV (2017) Cell death and cell lysis are separable events during pyroptosis. *Cell Death Discov* 3:17070.
20. Martín-Sánchez F, et al. (2016) Inflammasome-dependent IL-1β release depends upon membrane permeabilisation. *Cell Death Differ* 23:1219–1231.
21. Rühl S, Broz P (2015) Caspase-11 activates a canonical NLRP3 inflammasome by promoting K(+) efflux. *Eur J Immunol* 45:2927–2936.
22. Rayamajhi M, Zhang Y, Miao EA (2013) Detection of pyroptosis by measuring released lactate dehydrogenase activity. *Methods Mol Biol* 1040:85–90.
23. Fletcher DA, Mullins RD (2010) Cell mechanics and the cytoskeleton. *Nature* 463:485–492.
24. Brennan MA, Cookson BT (2000) Salmonella induces macrophage death by caspase-1-dependent necrosis. *Mol Microbiol* 38:31–40.
25. Byun Y, et al. (2001) Caspase cleavage of vimentin disrupts intermediate filaments and promotes apoptosis. *Cell Death Differ* 8:443–450.
26. Bonfoco E, et al. (1996) Cytoskeletal breakdown and apoptosis elicited by NO donors in cerebellar granule cells require NMDA receptor activation. *J Neurochem* 67:2484–2493.
27. Caulín C, Salvesen GS, Oshima RG (1997) Caspase cleavage of keratin 18 and reorganization of intermediate filaments during epithelial cell apoptosis. *J Cell Biol* 138: 1379–1394.
28. Lowery J, Kuczmarski ER, Herrmann H, Goldman RD (2015) Intermediate filaments play a pivotal role in regulating cell architecture and function. *J Biol Chem* 290: 17145–17153.
29. Moss DK, Betin VM, Malesinski SD, Lane JD (2006) A novel role for microtubules in apoptotic chromatin dynamics and cellular fragmentation. *J Cell Sci* 119:2362–2374.
30. Akhmanova A, Steinmetz MO (2015) Control of microtubule organization and dynamics: Two ends in the limelight. *Nat Rev Mol Cell Biol* 16:711–726.
31. Blanchoin L, Boujemaa-Paterski R, Sykes C, Plastino J (2014) Actin dynamics, architecture, and mechanics in cell motility. *Physiol Rev* 94:235–263.
32. Fischer S, Vandekerckhove J, Ampe C, Traub P, Weber K (1986) Protein-chemical identification of the major cleavage sites of the Ca2+ proteinase on murine vimentin, the mesenchymal intermediate filament protein. *Biol Chem Hoppe Seyler* 367:1147–1152.
33. Katsnelson MA, Rucker LG, Russo HM, Dubyak GR (2015) K+ efflux agonists induce NLRP3 inflammasome activation independently of Ca2+ signaling. *J Immunol* 194: 3937–3952.
34. Välimäki E, et al. (2016) Calpain activity is essential for ATP-driven unconventional vesicle-mediated protein secretion and inflammasome activation in human macrophages. *J Immunol* 197:3315–3325.
35. Dave JM, Bayless KJ (2014) Vimentin as an integral regulator of cell adhesion and endothelial sprouting. *Microcirculation* 21:333–344.
36. Papaioannou TG, Stefanadis C (2005) Vascular wall shear stress: Basic principles and methods. *Hellenic J Cardiol* 46:9–15.
37. Campàs O, et al. (2014) Quantifying cell-generated mechanical forces within living embryonic tissues. *Nat Methods* 11:183–189.
38. Maeda A, Fadeel B (2014) Mitochondria released by cells undergoing TNF-α-induced necroptosis act as danger signals. *Cell Death Dis* 5:e1312.
39. Lood C, et al. (2016) Neutrophil extracellular traps enriched in oxidized mitochondrial DNA are interferogenic and contribute to lupus-like disease. *Nat Med* 22:146–153.
40. Jorgensen I, Zhang Y, Krantz BA, Miao EA (2016) Pyroptosis triggers pore-induced intracellular traps (PITs) that capture bacteria and lead to their clearance by efferocytosis. *J Exp Med* 213:2113–2128.
41. Gross O, et al. (2012) Inflammasome activators induce interleukin-1α secretion via distinct pathways with differential requirement for the protease function of caspase-1. *Immunity* 36:388–400.
42. Russo HM, et al. (2016) Active caspase-1 induces plasma membrane pores that precede pyroptotic lysis and are blocked by lanthanides. *J Immunol* 197:1353–1367.
43. Salinas RE, et al. (2014) A cellular genome-wide association study reveals human variation in microtubule stability and a role in inflammatory cell death. *Mol Biol Cell* 25:76–86.
44. dos Santos G, et al. (2015) Vimentin regulates activation of the NLRP3 inflammasome. *Nat Commun* 6:6574.
45. Kahlenberg JM, et al. (2014) An essential role of caspase 1 in the induction of murine lupus and its associated vascular damage. *Arthritis Rheumatol* 66:152–162.
46. Suthar MS, Gale M, Jr, Owen DM (2009) Evasion and disruption of innate immune signalling by hepatitis C and West Nile viruses. *Cell Microbiol* 11:880–888.
47. Eckard SC, et al. (2014) The SKIV2L RNA exosome limits activation of the RIG-I-like receptors. *Nat Immunol* 15:839–845.
48. Gray EE, et al. (2016) The AIM2-like receptors are dispensable for the interferon response to intracellular DNA. *Immunity* 45:255–266.
49. Lood C, Arve S, Ledbetter J, Elkon KB (2017) TLR7/8 activation in neutrophils impairs immune complex phagocytosis through shedding of FcgRIIA. *J Exp Med* 214:2103–2119.
50. Lood C, Hughes GC (2017) Neutrophil extracellular traps as a potential source of autoantigen in cocaine-associated autoimmunity. *Rheumatology (Oxford)* 56:638–643.
51. Knez J, et al. (2017) Peripheral blood mitochondrial DNA content in relation to circulating metabolites and inflammatory markers: A population study. *PLoS One* 12:e0181036.
52. Jiang WW, et al. (2005) Increased mitochondrial DNA content in saliva associated with head and neck cancer. *Clin Cancer Res* 11:2486–2491.